DOI: https://doi.org/10.2138/am-2022-8056. http://www.minsocam.org/

Revision 2

Single-crystal elasticity of phase Egg $AlSiO_3OH$ and δ-AlOOH by Brillouin spectroscopy

Baoyun Wang[1,2,3], Yanyao Zhang[3], Suyu Fu[3,4], Wei Yan[5,6], Eiichi Takahashi[1,7], Li Li[1,7], Jung-Fu Lin [3*], Maoshuang Song[1,7*]

[1]State Key Laboratory of Isotope Geochemistry, Guangzhou Institute of Geochemistry, Chinese Academy of Sciences, Guangzhou 510640, China;

[2]College of Earth and Planetary Sciences, University of Chinese Academy of Sciences, Beijing, 100049, China;

[3]Department of Geological Sciences, Jackson School of Geosciences, The University of Texas at Austin, Austin, 78712 Texas, USA;

[4]School of Earth and Space Exploration, Arizona State University

[5]School of Earth and Space Sciences, Peking University, Beijing, 100871, China

[6]Key Laboratory of Orogenic Belts and Crustal Evolution, Ministry of Education of China, Beijing, 100871, China

[7]CAS Center for Excellence in Deep Earth Science, Guangzhou, 510640, China

[*]Corresponding email: afu@jsg.utexas.edu; msong@gig.ac.cn

Abstract

Phase Egg and δ-AlOOH are two typical hydrous phases that might exist in the wet sedimentary layer of subducted slabs under mantle conditions. They are thus regarded as potential water carriers to Earth's deep mantle. In this letter, we report the full elastic constants of both phases determined by Brillouin scattering and X-ray diffraction measurements under ambient conditions. Our results indicate that the hydrogen-bond configurations in the crystal structures of the two phases have a profound effect on their principal elastic constants. The adiabatic bulk modulus (K_S) and shear modulus (G) calculated from the obtained elastic constants using the Voigt-Reuss-Hill averaging scheme are 158.3(201) GPa and 123.0(60) GPa for phase Egg and 162.9(31) GPa and 145.2(13) GPa for δ-AlOOH, respectively. These results allow us to evaluate elastic moduli and sound velocities of hydrous minerals in the Al_2O_3-H_2O-SiO_2 ternary system (simplified composition of subducted wet sedimentary layer) at ambient conditions including the contrast of the acoustic velocities V_P and V_S for the reaction production $AlSi_3OH$=δ-AlOOH+SiO_2 (stishovite) and the evolution in the elastic moduli and sound velocities of hydrous minerals as a function of density.

Keywords: Phase Egg, δ-AlOOH, elasticity, anisotropy, Brillouin spectroscopy

Introduction

Hydrous phases which form in wet subducted lithospheric slabs are regarded as potential carriers for transporting water into the Earth's deep interior. Dehydration of these hydrous phases can release substantial amounts of water and significantly affect physical and chemical properties of the surrounding rocks, such as the rheology and electrical conductivity (Karato et al. 1986; Ohtani 2020). Researchers have examined phase relations in hydrous systems with various chemical compositions that are representative of sedimentary, basaltic and peridotitic layers of subducted slabs. These efforts have led to the discoveries of a number of hydrous minerals stable at relevant deep-mantle pressure-temperature conditions (Iwamori 2004; Litasov and Ohtani 2003; Schmidt and Poli 1998). Among these previously reported hydrous minerals in the simplified Al_2O_3-H_2O-SiO_2 ternary system, phase Egg and δ-AlOOH are two typical phases which might exist in the subducted wet sedimentary layer (Ono 1998; Schmidt et al. 1998). Experimental studies on the phase stability of phase Egg show that it remains stable at depths of the mantle transition zone even along a normal mantle geotherm. It then decomposes to δ-AlOOH and stishovite at greater depths in the topmost lower mantle (25-30 GPa) (Fukuyama et al. 2017; Pamato et al. 2015; Sano et al. 2004). δ-AlOOH is found to survive in the lower mantle down to core-mantle boundary conditions along a cold slab geotherm (Duan et al. 2018; Ohtani et al. 2001; Sano et al. 2008; Yuan et al. 2019). Therefore, phase Egg and δ-AlOOH can form a continuous chain to transport water from the mantle transition zone to the deep lower mantle through slab subduction processes. In addition, Wirth et al. (2007) claimed that phase Egg occurs as inclusions in ultradeep diamonds, providing geological evidence for the possible existence of phase Egg at the depth of the mantle transition zone.

Phase Egg with an ideal formula of $AlSiO_3OH$ was first synthesized by Eggleton et al. (1978). It is monoclinic system with space group $\boldsymbol{P}2_1/n$ (Schmidt et al. 1998) and consists of edge-shared Si-octahedra linked to an Al_2O_{10} dimer (Figure S1a and b). High-pressure X-ray diffraction studies show that the axial compressibility of phase Egg is extremely anisotropic (Schulze et al. 2018; Vanpeteghem et al. 2003), which is also supported by recent *first-principles* calculations (Mookherjee et al. 2019). δ-AlOOH is a synthetic high-pressure polymorph of diaspore (α-AlOOH) and boehmite (γ-AlOOH) that adopts a $CaCl_2$-type structure with $\boldsymbol{P}2_1nm$ space group (Figure S1c) (Suzuki et al. 2000). In recent years, δ-AlOOH has drawn increasing attention due to its pressure-induced hydrogen-bond symmetrization and wide P-T stability field (Hsieh et al. 2020; Sano-Furukawa et al. 2018; Sano-Furukawa et al. 2009). The formation of δ-phase AlOOH–FeOOH–$MgSiO_2(OH)_2$ solid solutions is of potential significance to deep-mantle water circulation and dynamic evolution (Yuan et al. 2019). Elastic data of phase Egg and δ-AlOOH are basic physical parameters and essential for interpreting seismic observations and probing the possible existence of these phases in the Earth. Although *first-principles* calculations have been performed to explore the elastic properties of these two phases (Mookherjee et al. 2019; Tsuchiya and Tsuchiya 2009), few experimental studies have reported their elastic constants even under ambient conditions. To date, only one Brillouin scattering study has been performed on δ-AlOOH polycrystalline aggregates (Mashino et al. 2016). Additionally, there are no available experimental elastic data for phase Egg with the exception of bulk modulus obtained from static compression X-ray diffraction experiments (Schulze et al. 2018; Vanpeteghem et al. 2003). Therefore, further experimental studies are required to shed new light on the elastic properties of these phases.

In this study, we performed Brillouin scattering and X-ray diffraction measurements on single-crystal phase Egg and δ-AlOOH under ambient conditions. The full elastic tensors were extracted by fitting measured acoustic velocities as a function of the phonon directions using the Christoffell's equation (Every 1980). We quantified the adiabatic bulk moduli (K_S), shear moduli (G), compressional-wave velocities (V_P) and shear-wave velocities (V_S) of phase Egg and δ-AlOOH under the Voigt-Reuss-Hill averaging scheme (Hill 1963). These results are compared with those of other typical hydrous minerals in the Al_2O_3-SiO_2-H_2O ternary system as a function of density to evaluate the correlation between these physical properties, compositions and crystal structures.

Experimental methods

Synthesis and characterization of single crystals

High-quality single crystals of phase Egg and δ-AlOOH were synthesized at high pressures and high temperatures using the Sakura 2500-ton multi-anvil apparatus at the Guangzhou Institute of Geochemistry, Chinese Academy of Sciences. To synthesize single-crystal phase Egg, a ground mixture of CaO, $Al(OH)_3$ and SiO_2 in a 1:4:2 mole ratio was used as the starting material and sealed in a welded gold capsule. The synthesis experiment was conducted at 17 GPa and 1400 °C with a duration of 20 hours (run number U801). The recovered products were composed of single crystals of phase Egg with maximum dimensions of 200 μm and some fine powders. The chemical compositions of several selected crystals were determined by electron microprobe analysis (EMPA) and are shown in Table S1. Based on these analyses, the crystals have an average of 50.5(1) wt% SiO_2 and 41.7(1) wt% Al_2O_3, yielding a chemical formula of $Al_{0.98}Si_{1.01}O_4H_{1.02}$ with the H content estimated by the total weight deficiency. This formula is close to the composition of the ideal formula of phase Egg. The products were also tested by single-crystal X-ray diffraction and unpolarized FTIR measurements. The single-crystal X-ray diffraction measurements were performed on a Bruker D8 Venture diffractometer equipped with a Mo *K*α radiation source (with a wavelength of 0.70926 Å), graphite monochromator, ω-scanning and Apex II CCD detector. These aforementioned characterizations confirm that the synthesized crystals are the phase Egg. The crystal structure was further refined using the Olex^2 package (Dolomanov et al. 2009) and the detail atomic parameters are available as a deposited CIF file. Unpolarized FTIR spectra in the range of 600–7500 cm^{-1} were recorded for several double-side polished crystals at ambient conditions using a Bruker Vertex 70 FTIR spectrometer combined with a

Hyperion-2000 IR microscope and a HgCdTe (MCT) detector (Figure S2). The spectra show three evident absorption bands centered at ~2140, ~2434 and ~2784 cm^{-1} (Figure S2), which could be assigned to be OH-stretching vibration of the phase Egg.

Single-crystal δ-AlOOH was synthesized by following the procedure reported by (Kawazoe et al. 2017). High-purity reagent-grade $Al(OH)_3$ powder of high purity (99.99%) was used as the starting material and the synthesis experiment was conducted at approximately 20 GPa and 1000 °C for a duration of 22 hours (run number U795). The recovered product is found to be composed of crystals with a maximum dimension of approximately 300 μm. Analyses of synchrotron X-ray diffraction patterns recorded at the 13-IDD beamline sector of GSECARS and EMPA measurements verify that the synthesized crystals are chemically homogeneous and pure δ-AlOOH phase (Figure S3 and Table S1).

Sample preparation and Brillouin scattering measurements

To precisely constrain the 13 and 9 elastic constants of phase Egg (monoclinic, $\boldsymbol{P}2_1/n$) and δ-AlOOH (orthorhombic, $\boldsymbol{P}2_1nm$), respectively, normally at least 3-4 platelets with different orientations are needed for Brillouin spectroscopic measurements. We carefully checked the synthesized crystals under a petrographic microscope and selected a number of high-quality clean and transparent crystals with homogeneous extinction for both phase Egg and δ-AlOOH. With the selected single crystals of phase Egg, we prepared four double-side polished platelets with ~15 μm thickness. To determine the crystallographic orientations and unit-cell parameters for all platelets, single-crystal X-ray diffraction measurements were performed using an Agilent SuperNova diffractometer (Atlas S2 CCD detector, Mo $K\alpha$ radiation, graphite monochromator) in the ω-scanning mode with the scanning step of 1° per frame. The scanning width varied from 80° to 100° and the exposure time varied from 7 s/° to15 s/° depending on the crystals. The obtained X-ray diffraction images were analysed using the CrysAlis Pro software (Oxford Diffraction 2006). The Miller indices of the polished platelets are determined to be (8, 3, -5), (0, -1, -1), (45, -6, 13) and (2, -1, 2) with an estimated uncertainty less than 0.2. All four crystal platelets display very similar lattice parameters and unit cell volumes, and the averaged values are a = 7.1449(7) Å, b = 4.3295(4) Å, c = 6.9526(7) Å, β = 98.35(9)° and V_0 = 201.79(4) Å^3, which are consistent with values reported by previous studies (Schulze et al. 2018; Vanpeteghem et al. 2003). The derived density is 3.740(2) g/cm^3 for phase Egg.

In the case of δ-AlOOH, it was difficult to prepare single-crystal platelets with ideal crystallographic orientations as the synthesized crystals were often twin crystals. Fortunately, some crystals were large enough to allow us to collect Brillouin scattering signals from one single-crystal domain. Finally, we obtained three workable platelets for Brillouin scattering measurements. The orientations and lattice parameters of these platelets were determined by single-crystal X-ray diffraction measurements at the 13-IDD beamline sector of GSECARS, Advanced Photon Source,

DOI: https://doi.org/10.2138/am-2022-8056. http://www.minsocam.org/

Argonne National Laboratory. The incident X-ray beam has an energy of 37 keV and a focused beam size of 3~4 μm at the sample. The geometry parameters were calibrated using LaB_6 standard. During X-ray diffraction measurements, the wide-scan images of the single crystal platelets were collected from -15° to +15° with the total exposure time of 100 s. The obtained diffraction patterns were analysed by GSE ADA/RSV software to derive crystallographic orientations (Dera et al. 2013). They were also integrated to one-dimensional profiles using Dioptas (Prescher and Prakapenka 2015). The Miller indices of the three platelets are determined to be (0, 0, 1), (2, 9, 2) and (10, 7, 3). The estimated accuracy of the measured Miller indices is within 0.1. The average lattice parameters of these three platelets are a = 4.7093(8) Å, b = 4.2271(1) Å, c = 2.8302(1) Å and V_0 = 56.34(5) Å^3, with a calculated density of 3.536(1) g/cm^3.

Brillouin scattering measurements were conducted under ambient conditions using a Brillouin Light Scattering (BLS) system at the Mineral Physics Laboratory, the University of Texas at Austin (Fu et al. 2017; Fu et al. 2019; Zhang et al. 2021). In the BLS system, a single-frequency 532 nm solid-state green laser (Coherent Verdi V2) was used as an excitation light source and a JRS six-pass tandem Fabry–Pérot interferometer equipped with a Perkin–Elmer photomultiplier detector was used to record the Brillouin spectra of the sample. Samples were loaded into a short-symmetrical diamond-anvil cell without a pressure transmitting medium. The laser beam was focused down to the sample with a spot size of approximately 20 μm in diameter. In a symmetric forward scattering geometry, acoustic velocities (v) were calculated from the measured Brillouin shifts (Δν) through the equation (Whitfield et al. 1976):

$$v = \frac{\Delta\nu \cdot \lambda_0}{2\sin(\theta/2)}$$

where v is the acoustic velocity, Δν is the measured Brillouin frequency shift, λ_0 is the laser wavelength of 532 nm, and θ is the external scattering angle of 48.3(1)° calibrated using water as a standard.

Results and discussion

Phase Egg

Brillouin scattering measurements were performed for each platelet of phase Egg in 19 distinct crystallographic directions by rotating the crystal in χ-circle over an angular range of 180° with an interval of 10°. One typical Brillouin spectrum is shown in Figure 1a. In most cases, both the compressional acoustic mode (V_P) and shear acoustic modes (V_{S1} and V_{S2}) can be observed, but the V_P signal overlaps with the strong V_S peak of diamond in some directions where only V_{S1} and V_{S2} were observed. The dispersion of the measured acoustic velocities with the crystallographic directions for the four platelets of phase Egg are depicted in Figure 2. Together with the density from the single-crystal X-ray diffraction and compositional measurements, the measured sound velocities are modelled to derive the 13 independent elastic constants of phase Egg by nonlinear least-squares fitting to Chritoffel's equation

(Every 1980). All the elastic constants C_{ij} based on the Cartesian coordinated system where the X-axis is parallel to the a^*-axis and Y-axis is parallel to the b-axis are given in Table 1 and compared with the theoretical values (Mookherjee et al. 2019). Our values are systematically lower than the theoretical values of Mookherjee et al. (2019). Although the reason for this discrepancy is unclear, one possible reason is thermal effects due to their *first-principles* calculations being performed at T=0 K (Mookherjee et al. 2019). Using the Voigt–Reuss–Hill averaging scheme (Hill 1963), aggregate properties such as K_S, G, V_P and V_S are also calculated and given in Table 1.

The principal elastic constants of phase Egg exhibit the relationship $C_{11}>C_{33}>C_{22}$, while the shear elastic components display the order $C_{55}>C_{66}>C_{44}$. These relations can be well explained by the orientation of the hydrogen bond, which is mostly aligned along the b-axis but tilted to have a component along the c-axis of the crystal structure. That is, the distortion of the SiO_6 octahedron with the longer Si-OH bond lies in the *a-c* plane (Schmidt et al. 1998; Schulze et al. 2018) (Figure S1a and b). The values of the principal elastic constants with C_{11} are twice as high as C_{22}, indicating that phase Egg has strikingly high anisotropy in the axial compressibility and that the b-axis is the most compressible direction. These observations are in agreement with previous static compression X-ray diffraction experiments (Schulze et al. 2018; Vanpeteghem et al. 2003).

The measured elastic constants of phase Egg allow us to evaluate the azimuthal anisotropy of the acoustic velocity. From 3D azimuthal images of the velocity distribution (Figure S4), we notice that the compressional-wave velocity varies from 7.68 km/s to 11.34 km/s. The fastest compressional-wave velocity propagates along the direction that deviates ~38° to the *a*-axis in the *a*-*c* plane, and the slowest compressional-wave velocity propagates along the *b*-axis direction. Similarly, the shear-wave velocity also exhibits a strong directional dependence. The anisotropy factors of the compressional-wave and shear-wave velocities, $AV=200\times(V_{max}-V_{min})/(V_{max}+V_{min})$, are calculated to be AV_P = 38.4% , AV_{S1} = 21.3% and AV_{S2} = 21.2% (Figure S4), and the shear-wave splitting factor, which is defined as $AV_S=200\times(V_{S1}-V_{S2})/(V_{S1}+V_{S2})$, is calculated to be 22.1% (Figure S4).

δ-AlOOH

Figure 1b shows a representative Brillouin spectrum of δ-AlOOH. The measured acoustic velocities as a function of the crystallographic directions for the three δ-AlOOH platelets are shown in Figure 3. The full 9 independent elastic constants of δ-AlOOH were inverted by fitting all the velocity data of the three platelets using Christoffel's equation and the results are given in Table 1. Our values of the elastic constants are comparable to the theoretical values from *first-principles* simulations (Tsuchiya and Tsuchiya 2009). We found that the principal elastic constants exhibit the relation $C_{33}>C_{11}>C_{22}$ and that C_{22} is much smaller than C_{33} and C_{11}. In accordance with this relation, the velocity along the *c*-axis is faster than those along the *a*-axis and *b*-axis by approximately 7.4% and 21.1%, respectively. The relation of $C_{33}>C_{11}>C_{22}$ is also reflected in the strong elastic anisotropy in the axial compressibility for δ-AlOOH, which is consistent with the fact that the O-H bond lies in the *a*-*b* plane (see Figure S1c). The compressibilities of the *a*- and the *b*-axes are higher than that of the *c*-axis. The anisotropic factors of δ-AlOOH are calculated to be AV_P = 19.1%, AV_{S1} = 6.89% and AV_{S2} = 6.56% (Figure S5). The shear-wave splitting factor is calculated to be AV_S = 12.65% (Figure S5). The calculated isotropic aggregate properties of δ-AlOOH are shown Table 1. Interestingly, we found that the aggregate V_P and V_S values in our study are 5.2% and 8.8% higher, respectively, than those determined by Mashino et al. (2016) using polycrystalline δ-AlOOH. Previous studies have shown that the grain size of the polycrystalline aggregate sample and volumetric fraction of grain boundaries significantly affect the obtained velocity in the Brillouin scattering measurements of MgO (Gleason et al. 2011; Marquardt et al. 2011). For example, Gleason et al. (2011) reported that the derived sound wave velocities of MgO powder compressed under nonhydrostatic conditions were lower than those of single-crystal MgO compressed under quasihydrostatic conditions. They proposed that the anomalously low velocities were related to the volume fraction of grain boundaries produced by crushed samples under nonhydrostatic conditions. Mashino et al. (2016) used fine-grained polycrystalline δ-AlOOH in their Brillouin measurements under ambient conditions. Based on the difference in experimental conditions, the discrepancy between our results and those of Mashino et al. (2016) can be contributed to the grain size and grain boundary effects in the polycrystalline samples. Future systematic studies are needed to clarify this issue.

Implications

The combination of seismic observations of the deep mantle and elastic results of water-bearing or hydrous minerals can be an effective means to elucidate the water storage, distribution and circulation in the Earth's interior. We compiled the density, aggregate elastic moduli, aggregate acoustic velocities and anisotropy factors of typical mantle minerals in subducted slabs, and compare them with those of phase Egg and δ-AlOOH under ambient conditions (Table S2). The AV_P and AV_S values of phase Egg are higher than those of most other minerals, such as olivine, diopside and wadsleyite; hence, phase Egg is likely a candidate mineral for seismic anisotropy in subducting slabs. The acoustic velocities (V_P and V_S) of phase Egg are remarkably higher than those of the major minerals in the upper mantle (olivine, enstatite, diopside and majorite), but comparable to those of the minerals in the mantle transition zone (wadsleyite and ringwoodite). The acoustic velocities of δ-AlOOH are faster than those of all the minerals in the mantle transition zone and the upper mantle but slower than those of the major lower-mantle mineral bridgmanite. Thus, phase Egg may result in a high-velocity anomaly at the depth of the base of the upper mantle, while δ-AlOOH may result in a high-velocity anomaly at the depth of the mantle transition zone. As mentioned before, phase Egg decomposes to δ-AlOOH and stishovite through the $AlSi_3OH$=δ-AlOOH+SiO_2 reaction at relevant P-T conditions of the topmost lower mantle along the slab geotherm. Based on the elastic data obtained under ambient conditions in this study, the velocity contrast of this reaction

DOI: https://doi.org/10.2138/am-2022-8056. http://www.minsocam.org/

is determined to be ~17% for V_P and ~18% for V_S, which is likely detectable by regional high-resolution seismic tomography. We note that the discussion above is based on elastic data obtained under ambient conditions and the effects of pressure and temperature on the elasticity of these phase remain to be investigated in the future. As hydrogen-bond configurations and pressure-induced hydrogen-bond evolution have profound effects on the elastic properties of phase Egg and δ-AlOOH (Mookherjee et al. 2019; Tsuchiya and Tsuchiya 2009), future high pressure experimental investigations on the elasticity of these two phases are thus critically needed.

To systematically understand the elastic properties of hydrous minerals in the sedimentary layer of subducted slabs, we have plotted the K_S, G, V_P and V_S of hydrous minerals in the Al_2O_3-SiO_2-H_2O ternary system as a function of density (Figure 4). The K_S, G, V_P and V_S values of these hydrous minerals, including kaolinite, phase pi, diaspore, topaz and δ-AlOOH, exhibit a positive linear relationship with the density. Such linear relationships are also observed for the phases along the forsterite-brucite join of the MgO-SiO_2-H_2O ternary system. However, the K_S, G, V_P and V_S values of phase Egg significantly deviate from the linear trends with slightly lower values than those predicted by the linear relationships, showing anomalous elastic behavior probably due to hydrogen-bond configurations in its crystal structure.

Acknowledgments

We thank Vincent Lynch at University of Texas X-ray Diffraction Lab for measuring the crystallographic orientations of the phase Egg. The single-crystal X-ray diffraction measurements of δ-AlOOH were performed at GSECARS, Advanced Photon Source, Argonne National Laboratory. GSECARS is supported by the National Science Foundation-Earth Sciences (EAR-1634415) and Department of Energy-GeoSciences (DEFG02-94ER14466). This research at Guangzhou Institute of Geochemistry is financially supported by the Strategic Priority Research Program (B) of the Chinese Academy of Sciences (Grant No. XDB18000000) and the National Natural Science Foundation of China (Grant No. 41874107 and 41574079). J.F.L. acknowledges support from the Geophysics Program of the National Science Foundation, U.S. (EAR-1916941 and EAR-2001381).

References

Dera, P., Zhuravlev, K., Prakapenka, V., Rivers, M.L., Finkelstein, G.J., Lavina, B., Grubor-Urosevic, O., Tschauner, O., Clark, S.M., and Downs, R.T. (2013) High pressure single-crystal micro X-ray diffraction analysis with GSE_ADA/ RSV software. High Pressure Research, 34, 1–19.

Dolomanov, O.V., Bourhis, L.J., Gildea, R.J., Howard, J.A.K., and Puschmann, H. (2009) OLEX2: a complete structure solution, refinement and analysis program. Journal of Applied Crystallography, 42, 339–341

Duan, Y., Sun, N., Wang, S., Li, X., Guo, X., Ni, H., Prakapenka, V.B., and Mao, Z. (2018) Phase stability and thermal equation of state of δ-AlOOH: Implication for water transportation to the Deep Lower Mantle. Earth and Planetary Science Letters, 494, 92-98.

Eggleton, R.A., Boland, J.N., and Ringwood, A.E. (1978) High-pressure synthesis of a new aluminum silicate-$Al_5Si_5O_{17}(OH)$. Geochemical Journal, 12(3), 191-194.

Every, A. (1980) General closed-form expressions for acoustic waves in elastically anisotropic solids. Physical Review B, 22(4), 1746.

Fu, S., Yang, J., and Lin, J.-F. (2017) Abnormal elasticity of single-crystal magnesiosiderite across the spin transition in Earth's lower mantle. Physical review letters, 118(3), 036402.

Fu, S., Yang, J., Tsujino, N., Okuchi, T., Purevjav, N., and Lin, J.-F. (2019) Single-crystal elasticity of (Al,Fe)-bearing bridgmanite and seismic shear wave radial anisotropy at the topmost lower mantle. Earth and Planetary Science Letters, 518, 116-126.

Fukuyama, K., Ohtani, E., Shibazaki, Y., Kagi, H., and Suzuki, A. (2017) Stability field of phase Egg, $AlSiO_3OH$ at high pressure and high temperature: possible water reservoir in mantle transition zone. Journal of Mineralogical and Petrological Sciences, 112(1), 31-35.

Gleason, A.E., Marquardt, H., Chen, B., Speziale, S., Wu, J., and Jeanloz, R. (2011) Anomalous sound velocities in polycrystalline MgO under non-hydrostatic compression. Geophysical Research Letters, 38.

Hill, R. (1963) Elastic properties of reinforced solids: some theoretical principles. Journal of the Mechanics and Physics of Solids, 11, 357–372

Hsieh, W.P., Ishii, T., Chao, K.H., Tsuchiya, J., Deschamps, F., and Ohtani, E. (2020) Spin transition of iron in δ-(Al,Fe)OOH induces thermal anomalies in Earth's lower mantle. Geophysical Research Letters, 47(4), e2020GL087036.

Iwamori, H. (2004) Phase relations of peridotites under H_2O-saturated conditions and ability of subducting plates for transportation of H_2O. Earth and Planetary Science Letters, 227(1-2), 57-71.

Jiang, F., Majzlan, J., Speziale, S., He, D., and Duffy, T.S. (2008) Single-crystal elasticity of diaspore, AlOOH, to 12 GPa by Brillouin scattering. Physics of the Earth and Planetary Interiors, 170(3-4), 221-228.

Karato, S.I., Paterson, M.S., and FitzGerald, J.D. (1986) Rheology of synthetic olivine aggregates: Influence of grain size and water. Journal of Geophysical Research: Solid Earth, 91(B8), 8151-8176.

Katahara, K.W. (1996) Clay mineral elastic properties. SEG Technical Program Expanded Abstracts, 1691-1694. DOI: http://dx.doi.org/10.1190/1.1826454.

Kawazoe, T., Ohira, I., Ishii, T., Ballaran, T.B., McCammon, C., Suzuki, A., and Ohtani, E. (2017) Single crystal synthesis of δ-(Al,Fe)OOH. American Mineralogist, 102(9), 1953-1956.

Litasov, K., and Ohtani, E. (2003) Stability of various hydrous phases in CMAS pyrolite-H_2O system up to 25 GPa. Physics and Chemistry of Minerals, 30(3), 147-156.

Marquardt, H., Gleason, A., Marquardt, K., Speziale, S., Miyagi, L., Neusser, G., Wenk, H.R., and Jeanloz, R. (2011) Elastic properties of MgO nanocrystals and grain boundaries at high pressures by Brillouin scattering. Physical Review B, 84(6).

Mashino, I., Murakami, M., and Ohtani, E. (2016) Sound velocities of δ-AlOOH up to core-mantle boundary pressures with implications for the seismic anomalies in the deep mantle. Journal of Geophysical Research: Solid Earth, 121(2), 595-609.

Mookherjee, M., Panero, W.R., Wunder, B., and Jahn, S. (2019) Anomalous elastic behavior of phase egg, $AlSiO_3(OH)$, at high pressures. American Mineralogist, 104(1), 130-139.

Mookherjee, M., Tsuchiya, J., and Hariharan, A. (2016) Crystal structure, equation of state, and elasticity of hydrous aluminosilicate phase, topaz-OH ($Al_2SiO_4(OH)_2$) at high pressures. Physics of the Earth and Planetary Interiors, 251, 24-35.

Ohtani, E. (2020) The role of water in Earth's mantle. National Science Review, 7(1), 224-232.

Ohtani, E., Litasov, K., Suzuki, A., and Kondo, T. (2001) Stability field of new hydrous phase, δ-AlOOH, with implications for water transport into the deep mantle. Geophysical Research Letters, 28(20), 3991-3993.

Ono, S. (1998) Stability limits of hydrous minerals in sediment and mid-ocean ridge basalt compositions: Implications for water transport in subduction zones. Journal of Geophysical Research-Solid Earth, 103(B8), 18253-18267.

Oxford Diffraction (2006) CrysAlis Software system, Version 171.35.19. Oxford Diffraction Ltd., Xcalibur CCD system.

Pamato, M.G., Myhill, R., Ballaran, T.B., Frost, D.J., Heidelbach, F., and Miyajima, N. (2015) Lower-mantle water reservoir implied by the extreme stability of a hydrous aluminosilicate. Nature Geoscience, 8(1), 75-79.

Peng, Y., Mookherjee, M., Hermann, A., Bajgain, S., Liu, S., and Wunder, B. (2017) Elasticity of phase-Pi ($Al_3Si_2O_7(OH)_3$)–A hydrous aluminosilicate phase. Physics of the Earth and Planetary Interiors, 269, 91-97.

Prescher, C., and Prakapenka, V.B. (2015) DIOPTAS: A program for reduction of two-dimensional X-ray diffraction data and data exploration. High Pressure Research, 35, 223–230.

Sano-Furukawa, A., Hattori, T., Komatsu, K., Kagi, H., Nagai, T., Molaison, J.J., dos Santos, A.M., and Tulk, C.A. (2018) Direct observation of symmetrization of hydrogen bond in δ-AlOOH under mantle conditions using neutron diffraction. Scientific reports, 8(1), 1-9.

Sano-Furukawa, A., Kagi, H., Nagai, T., Nakano, S., Fukura, S., Ushijima, D., Iizuka, R., Ohtani, E., and Yagi, T. (2009) Change in compressibility of δ-AlOOH and δ-AlOOD at high pressure: A study of isotope effect and hydrogen-bond symmetrization. American Mineralogist, 94(8-9), 1255-1261.

Sano, A., Ohtani, E., Kondo, T., Hirao, N., Sakai, T., Sata, N., Ohishi, Y., and

Kikegawa, T. (2008) Aluminous hydrous mineral δ-AlOOH as a carrier of hydrogen into the core-mantle boundary. Geophysical Research Letters, 35(3).

Sano, A., Ohtani, E., Kubo, T., and Funakoshi, K.-i. (2004) In situ X-ray observation of decomposition of hydrous aluminum silicate $AlSiO_3OH$ and aluminum oxide hydroxide δ-AlOOH at high pressure and temperature. Journal of Physics and Chemistry of Solids, 65(8-9), 1547-1554.

Schmidt, M.W., Finger, L.W., Angel, R.J., and Dinnebier, R.E. (1998) Synthesis, crystal structure, and phase relations of $AlSiO_3OH$, a high-pressure hydrous phase. American Mineralogist, 83(7-8), 881-888.

Schmidt, M.W., and Poli, S. (1998) Experimentally based water budgets for dehydrating slabs and consequences for arc magma generation. Earth and Planetary Science Letters, 163(1-4), 361-379.

Scholtzová, E., and Tunega, D. (2020) Prediction of mechanical properties of grafted kaolinite–A DFT study. Applied Clay Science, 193, 105692.

Schulze, K., Pamato, M.G., Kurnosov, A., Ballaran, T.B., Glazyrin, K., Pakhomova, A., and Marquardt, H. (2018) High-pressure single-crystal structural analysis of $AlSiO_3OH$ phase egg. American Mineralogist, 103(12), 1975-1980.

Suzuki, A., Ohtani, E., and Kamada, T. (2000) A new hydrous phase δ-AlOOH synthesized at 21 GPa and 1000 °C. Physics and Chemistry of Minerals, 27(10), 689-693.

Tennakoon, S., Peng, Y., Mookherjee, M., Speziale, S., Manthilake, G., Besara, T., Andreu, L., and Rivera, F. (2018) Single crystal elasticity of natural topaz at high-temperatures. Scientific reports, 8(1), 1-9.

Tsuchiya, J., and Tsuchiya, T. (2009) Elastic properties of δ-AlOOH under pressure: First principles investigation. Physics of the Earth and planetary interiors, 174(1-4), 122-127.

Vanpeteghem, C.B., Ohtani, E., Kondo, T., Takemura, K., and Kikegawa, T. (2003) Compressibility of phase Egg $AlSiO_3OH$: Equation of state and role of water at high pressure. American Mineralogist, 88(10), 1408-1411.

Whitfield, C.H., Brody, E.M., and Bassett, W.A. (1976) Elastic moduli of NaCl by Brillouin scattering at high pressure in a diamond anvil cell. Review of Scientific Instruments, 47(8), 942-947.

Wirth, R., Vollmer, C., Brenker, F., Matsyuk, S., and Kaminsky, F. (2007) Inclusions of nanocrystalline hydrous aluminium silicate "Phase Egg" in superdeep diamonds from Juina (Mato Grosso State, Brazil). Earth and Planetary Science Letters, 259(3-4), 384-399.

Yuan, H., Zhang, L., Ohtani, E., Meng, Y., Greenberg, E., and Prakapenka, V.B. (2019) Stability of Fe-bearing hydrous phases and element partitioning in the system $MgO–Al_2O_3–Fe_2O_3–SiO_2–H_2O$ in Earth's lowermost mantle. Earth and Planetary Science Letters, 524, 115714.

Zhang, Y., Fu, S., Wang, B., and Lin, J.-F. (2021) Elasticity of a Pseudoproper Ferroelastic Transition from Stishovite to Post-Stishovite at High Pressure.

Physical Review Letters, 126(2), 025701.

Tables

Table 1. Elastic properties of phase Egg and δ-AlOOH under ambient conditions.

	Phase Egg		δ-AlOOH		
	Experiment	Calculation	Experiment	Experiment	Calculation
	Single-crystal	-	Single-crystal	Polycrystal	-
	This study	Mookherjee et al. (2019)	This study	Mashino et al. (2015)	Tsuchiya and Tsuchiya (2009)
ρ (g/cm^3)	3.740(2)	3.798	3.536(1)		3.383
C_{11} (GPa)	467.2(15)	504.7	375.9(9)		314
C_{22} (GPa)	220.8(8)	280.4	295.4(11)		306
C_{33} (GPa)	305.2(7)	401.0	433.5(12)		391
C_{44} (GPa)	109.8(4)	150.3	129.2(6)		117
C_{55} (GPa)	166.0(5)	174.0	133.4(7)		115
C_{66} (GPa)	139.6(5)	159.7	166.4(6)		152
C_{12} (GPa)	115.9(9)	98.6	49.7(9)		34
C_{13} (GPa)	164.3(9)	141.6	91.9(15)		95
C_{23} (GPa)	26.3(7)	87.9	52.8(21)		67

DOI: https://doi.org/10.2138/am-2022-8056. http://www.minsocam.org/

C_{15} (GPa)	3.2(6)	7.5			
C_{25} (GPa)	20.9(9)	13.5			
C_{35} (GPa)	21.2(4)	19.8			
C_{46} (GPa)	13.7(4)	18.6			
K_{Voigt} (GPa)	178.5(8)	204.7	166.0(13)		155.9
G_{Voigt} (GPa)	128.9(3)	154.0	146.5(3)		131.1
K_{Reuss} (GPa)	138.2(46)	188.2	159.8(48)		151.2
G_{Reuss} (GPa)	117.0(17)	148.4	144.0(15)		128.8
K_{VRH} (GPa)	158.3(201)	196.4	162.9(31)		153.5
G_{VRH} (GPa)	123.0(60)	151.2	145.2(13)		130.0
V_{P} (km/s)	9.28(41)	10.25	10.04(7)	9.54(7)	9.83
V_{S} (km/s)	5.73(14)	6.32	6.41(3)	5.89(10)	6.20

Figure captions

Figure 1. Representative Brillouin spectra of (a) phase Egg and (b) δ-AlOOH at ambient conditions. V_P, V_{S1}, and V_{S2} peaks are observed in both crystals. The Miller indices of each crystal platelet is shown at the top-right corner of the panel.

Figure 2. Measured velocities of single-crystal phase Egg as a function of χ angle in the crystallographic plane. The Miller indices of the crystal platelets are shown in the panels. The dashed lines are calculated velocity dispersion curves using the fitted

DOI: https://doi.org/10.2138/am-2022-8056. http://www.minsocam.org/

elastic constants of the crystal.

Figure 3. Measured velocities of single-crystal δ-AlOOH as a function of χ angle in the crystallographic plane. The Miller indices of the crystal platelets are shown in the panels. The dashed lines are calculated velocity dispersion curves using the fitted elastic constants of the crystal.

Figure 4. Elastic moduli and sound velocities of hydrous minerals in the Al_2O_3-H_2O-SiO_2 ternary system at ambient conditions. These minerals include kl=kaolinite (Katahara 1996; Scholtzová and Tunega 2020), dia=diaspore (Jiang et al. 2008), pi=phase pi (Peng et al. 2017), top=topaz (Mookherjee et al. 2016; Tennakoon et al. 2018), δ=δ-AlOOH (Tsuchiya and Tsuchiya 2009; this study) and egg=phase Egg (Mookherjee et al. 2019; this study). (a) and (b) Adiabatic bulk moduli and shear moduli. (c) and (d) Compressional wave velocities and shear wave velocities. The square and circle symbols represent experimental data and theoretical data, respectively. The dashed lines are linear fitting results of all the data with the exception of phase Egg and the formulas are shown near the lines.

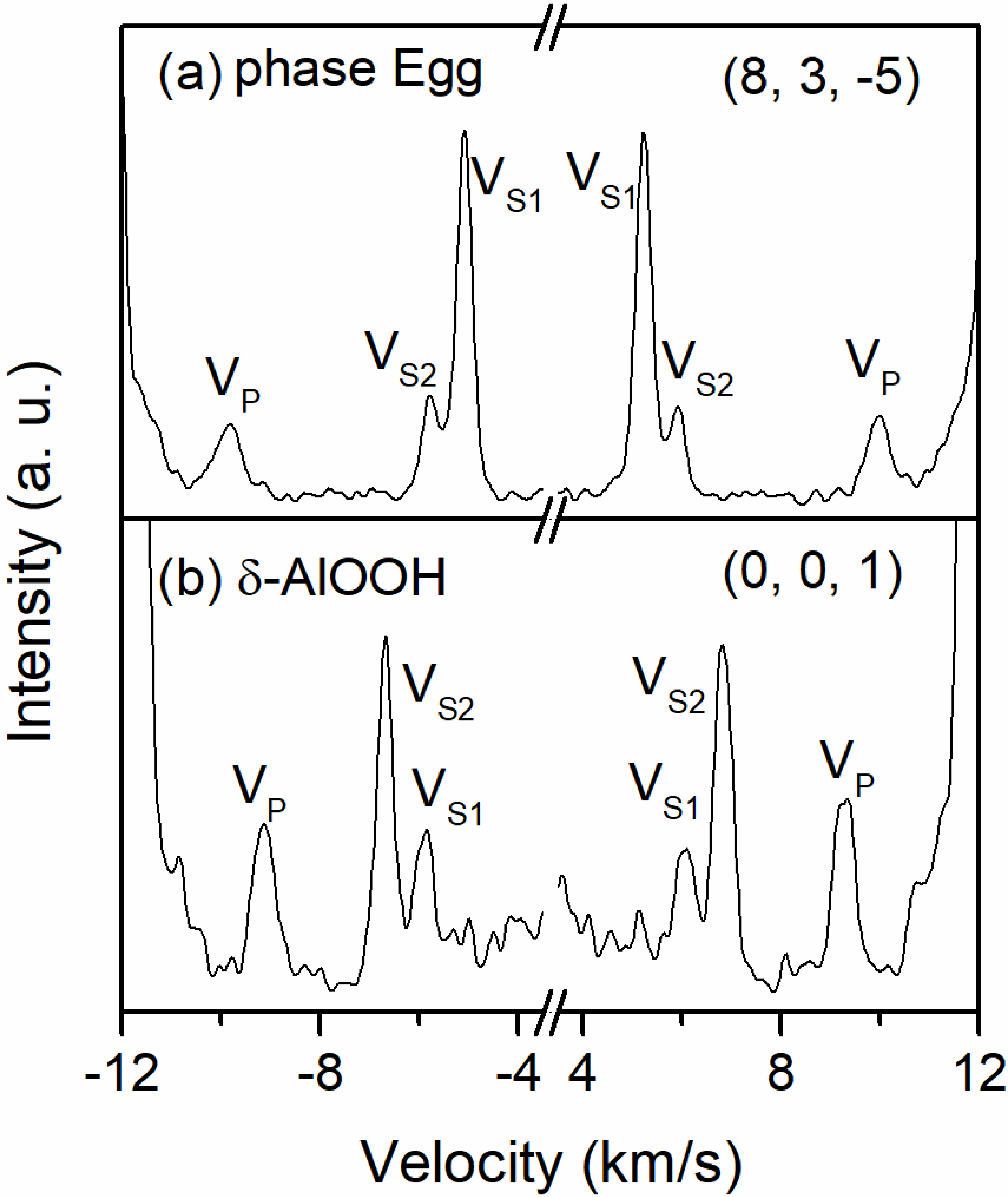

(a) phase Egg
(8, 3, -5)
V_P
V_S2
V_S1
V_S1
V_S2
V_P
(b) δ-AlOOH
(0, 0, 1)
V_P
V_S2
V_S1
V_S2
V_S1
V_P
Intensity (a. u.)
-12
-8
-4
4
8
12
Velocity (km/s)

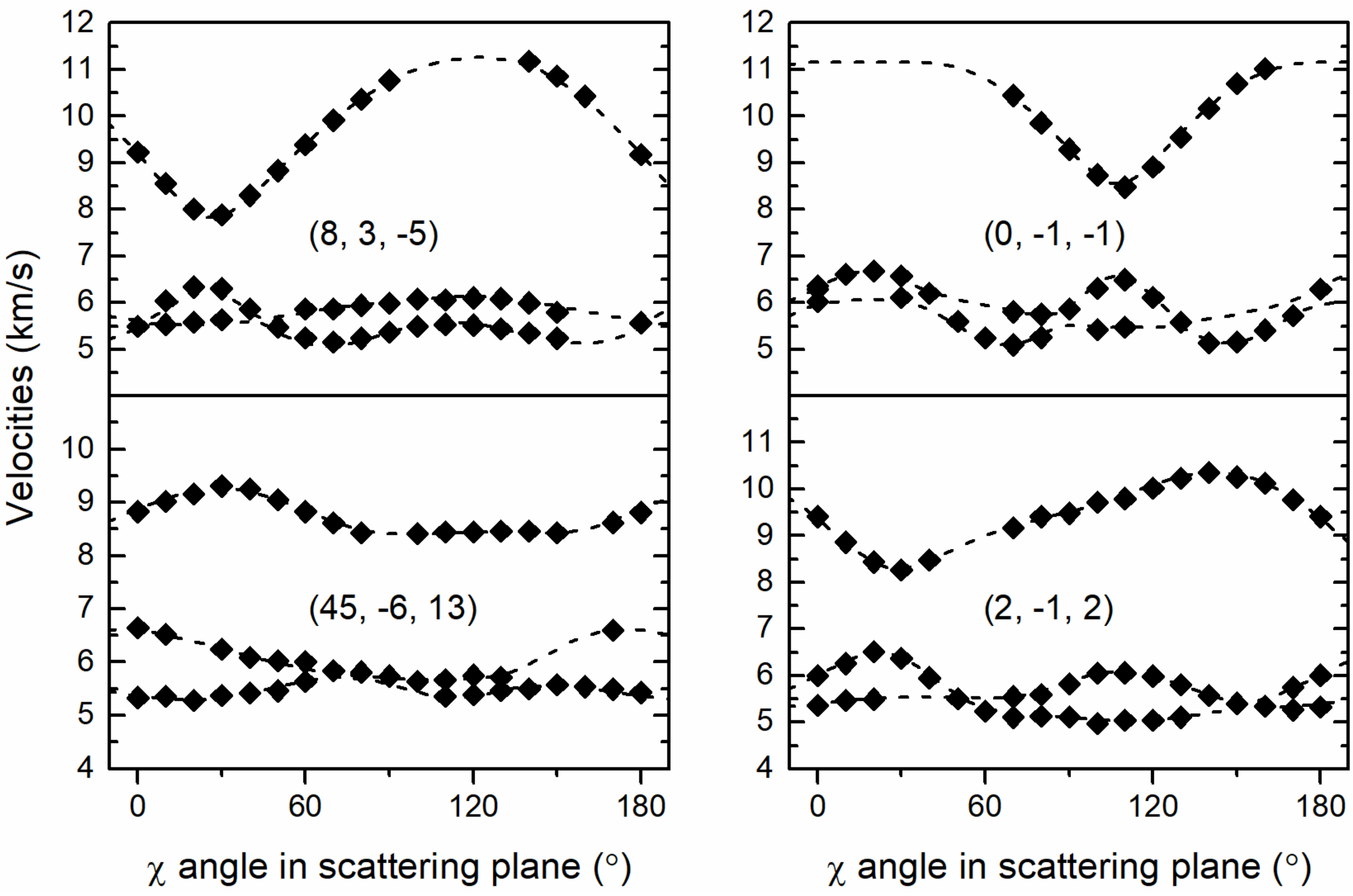
Velocities (km/s)
(8, 3, -5)
(0, -1, -1)
(45, -6, 13)
(2, -1, 2)
χ angle in scattering plane (°)
χ angle in scattering plane (°)

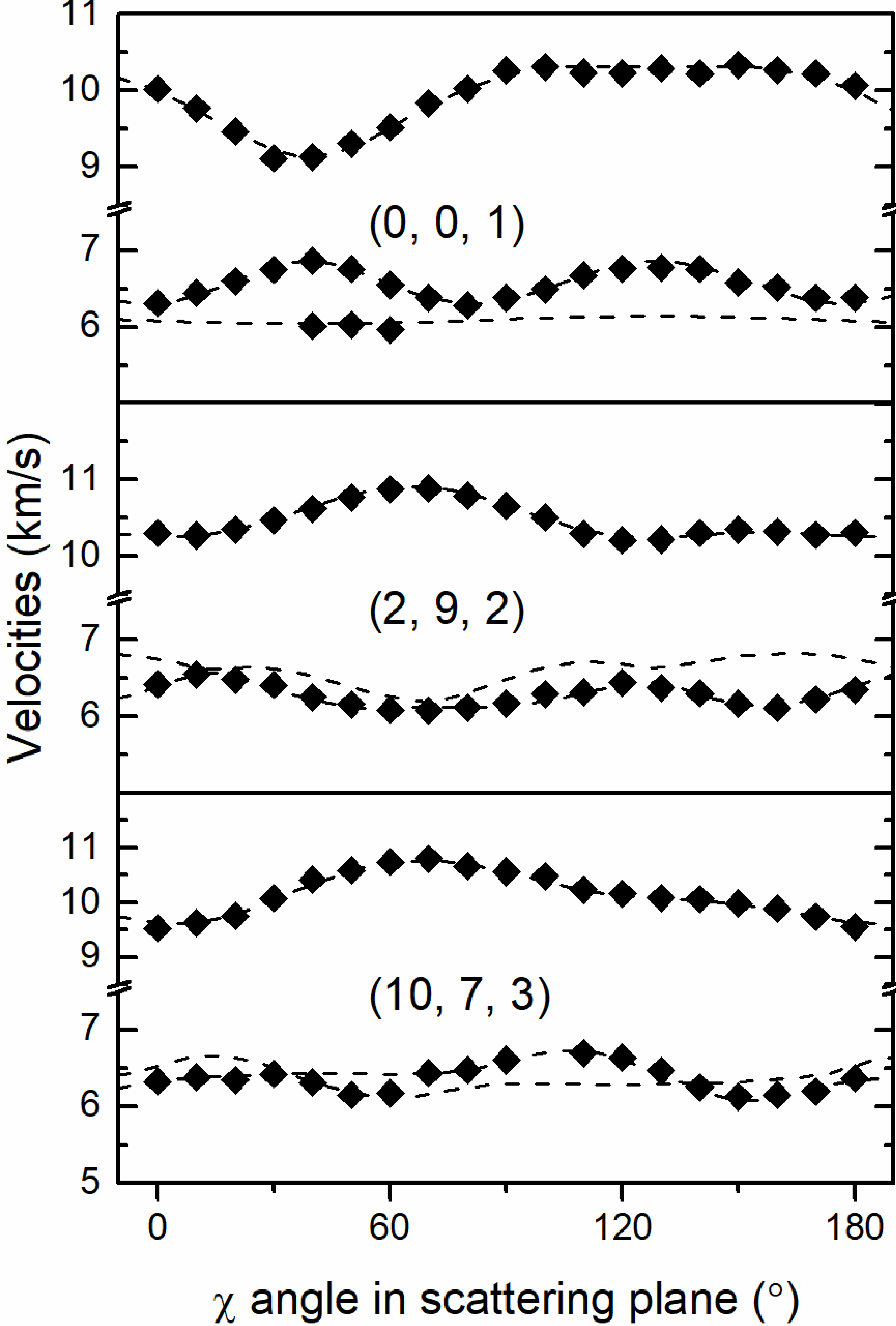

Velocities (km/s)
(0, 0, 1)
(2, 9, 2)
(10, 7, 3)
χ angle in scattering plane (°)

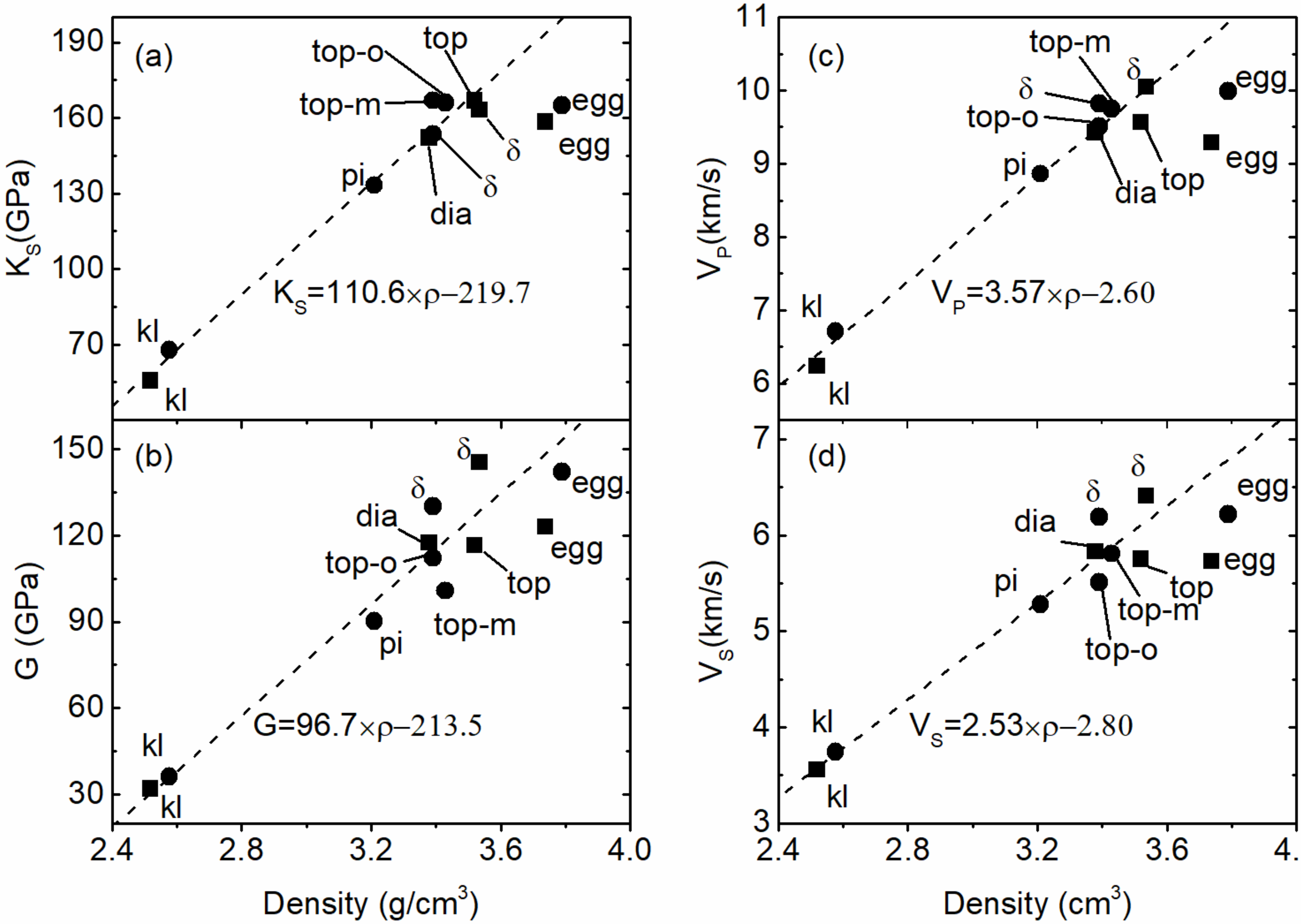

(a)
(b)
(c)
(d)
K_S(GPa)
G (GPa)
V_P(km/s)
V_S(km/s)
Density (g/cm^3)
Density (cm^3)
K_S=110.6×ρ−219.7
G=96.7×ρ−213.5
V_P=3.57×ρ−2.60
V_S=2.53×ρ−2.80
top-o
top-m
top
δ
dia
pi
egg
kl